Journal of Energy, Environmental & Chemical Engineering
2022; 7(3): 54-65
http://www.sciencepublishinggroup.com/j/jeece
doi: 10.11648/j.jeece.20220703.12
ISSN: 2637-4331 (Print); ISSN: 2637-434X (Online)

Synthesis and Characterization of MgO-Doped / Acid Modified Metakaolin Supported Ni-Based Catalysts

Abdullahi Nwaha Isah[1, 2, *], Elizabeth Jumoke Eterigho[2], Moses Aderemi Olutoye[2], Mohammed Umar Garba[2]

[1]Department of Chemical Engineering Technology, School of Engineering Technology, Federal Polytechnic Nasarawa, Nasarawa, Nigeria

[2]Department of Chemical Engineering, School of Infrastructure, Process Engineering and Technology, Federal University of Technology, Minna, Nigeria

Email address:

isnab2006@yahoo.com (A. N. Isah)

[*]Corresponding author

To cite this article:

Abdullahi Nwaha Isah, Elizabeth Jumoke Eterigho, Moses Aderemi Olutoye, Mohammed Umar Garba. Synthesis and Characterization of MgO-Doped / Acid Modified Metakaolin Supported Ni-Based Catalysts. *Journal of Energy, Environmental & Chemical Engineering.* Vol. 7, No. 3, 2022, pp. 54-65. doi: 10.11648/j.jeece.20220703.12

Received: October 21, 2021; **Accepted**: November 15, 2021; **Published**: July 13, 2022

Abstract: Catalytic steam reforming of bioethanol is an endothermic reaction for hydrogen production with high tendency of complete conversion at high temperature, but the catalyst is susceptible to deactivation due to the sintering of based metal and carbon deposition. MgO-doped/acid modified metakaolin supported nickel-based catalysts (with 5-25wt% nickel loading) were synthesized using wetness impregnation method and characterized. The physicochemical properties of the catalysts were examined using XRD, BET, SEM-EDX, XRF, FTIR and TG/DTA techniques. XRD patterns show the presence of nickel oxide, spinel $MgAl_2O_4$, $NiAl_2O_4$ in all the calcined catalyst samples, via characteristic peaks. Most of the crystallite sizes of the NiO particles in the synthesized catalysts were within 20.1-38nm, far less than the size effect threshold of 100nm, except CAT II, with crystallite size of 132.5nm, which could be attributed to the high tendency of NiO particles to agglomerate with MgO. Based on BET results, all the synthesized catalysts have pore diameter in the mesopore diameter range. SEM-EDX results show that there is nuclear interaction among MgO, NiO and Al_2O_3, as confirmed by XRD and XRF analyses. The FTIR analyses show that nickel phyllosilicate bond, Si-O-Al stretching vibration, OH stretching and metal-oxygen bond exist within the synthesized catalysts. The formation of $MgAl_2O_4$ and $NiAl_2O_4$ spinel phases is due to the interaction of active oxide components with acid modified metakaolin and MgO, which contributes to the catalyst thermal stability, as confirmed by TG/DTA analyses. These spinel structures would contribute to the catalysts' activity and selectivity, as their structures could remain unchanged under severe reaction conditions. The mesoporous structure of the synthesized catalysts would aid the reactant gases to adsorb on its surface and easy diffusion through the catalyst's channel after reaction. With better interaction among the support, promoter and based metal in the synthesized catalysts and available surface OH group, the formation and conversion of adsorbed formate intermediate during steam reforming reactions would be facilitated, and in turn reduce carbon deposition.

Keywords: Synthesis, Catalyst, Impregnation, Physicochemical, Reforming, Carbon Deposition

1. Introduction

The profuse release of greenhouse gases to the atmosphere due to over dependence on fossil fuel for the provision of end-use services and the need for energy sustainability due to the finite nature of carbon-fuel, necessitate the clamour for alternative energy sources that are green and sustainable [1, 2]. Renewable energy resources such as solar, wind, geothermal and biomass have gained attention as carbon neutral in relation to environmental impacts compared with fossil fuels [3]. Biomass has comparatives advantages over other renewable energy resources due to its abundant availability at low cost from different sources such as agriculture and forestry residuals, energy crops, aquatic plants, algae, lignocellulose materials, municipal and industrial wastes. Biomass reduces air pollution by reducing carbon dioxide by 90% through the photosynthesis process compared with fossil fuels [4].

Biomass can be transformed into energy through biological, thermal and chemical processes. Pyrolysis, gasification and steam gasification techniques are available for converting biomass to a useful form of energy, but there is concern about high tendencies of global warming, which necessitates research interest in the development of environmental benign biological methods for hydrogen production from biomass [5]. Biological hydrogen production can be achieved by photolysis, photofermentation and dark fermentation bacteria and anaerobic fermentative bacteria, respectively. Although, each of the production methods has its comparative advantages and disadvantages, fermentative hydrogen production has gained wider interest because there is high tendency of effective conversion of biomass (lignocellulose) to fermentable sugars during hydrolysis and onward fermentation into dilute bioethanol [6]. Bioethanol is an oxygenated fuel that contains 35% oxygen, which has gained attention for hydrogen production because of its relatively high hydrogen content, eco-friendly, as well as better safety in terms of storage and handling [7, 8]. Steam reforming, partial oxidation and auto thermal reforming are the prevalent, effective and large scale production methods of hydrogen from bio-ethanol. Among the reforming methods, steam reforming is one of the most widely studied routes of producing hydrogen because of its high efficiency (≈70-80%), low operational, production costs, and it guarantees high hydrogen yield [9]. In steam reforming, bulk metals, and mixed metal oxides are respectively used as catalysts. Among the bulk metals, nickel, copper, and cobalt are mostly used as catalysts in the ethanol steam reforming process because of their good catalytic activity, low cost and easy regeneration. Nickel and cobalt (Ni and Co) perform excellently in the cleavage of C-C, C-H and C-O [10, 11]. Nickel is prioritized due to its high activity for C-C bond and O-H bond breaking and its influence on the formation of molecular hydrogen but is susceptible to sintering and carbon deposition. This defect can be reduced by modifying the catalyst with support, due to their chemical effect, apart from their interaction with the active phase [12, 13]. Supported nickel catalysts provide good activity and high selectivity to hydrogen and COx. Support containing SiO_2 and/or γ-Al_2O_3 provides control of the Ni particle size and prevents sintering under reaction conditions owing to a confinement of the metal particles within structural pores, thus ensuring a high catalyst stability [14]. The use of catalytic metal (Ni and Co) supported on various oxides (SiO_2, Al_2O_3, CeO_2, ZrO_2 and MgO) has been tested in the reactions of decomposition of ethanol to produce hydrogen and carbon nanotubes [15]. Ni supported on SiO_2 exhibits high surface area, but when it is exposed to high temperature in the presence of steam, it may aggregate and cause loss of activity. Alkaline earth metals (MgO and CaO) have been used to modify Ni-based catalysts, in order to increase their activity, reducibility, stability, regenerability and decrease the coke formation rate. In particular, MgO favours water adsorption and OH mobility on the surface enhancing coke gasification and adjust the syngas composition using lattice oxygen [16]. NiO and MgO can form theoretically ideal solid solution in any molar ratio and strong interaction between them helps in preventing Ni particle sintering and the coke dispersion [17, 14]. Using porous support with an adequate pore texture and high surface area, it eliminates diffusional limitations that are often encountered during fluid-solid catalyst interaction and increase its resistance against sintering [18, 19]. In supported catalysts, controlling metal-support interactions is one of the most important strategies to tune catalytic properties in heterogeneous catalysis, especially their reactivity, selectivity, stability and in turn the identification of reaction mechanisms [20, 21]. Effective supports for steam reforming catalysts could be synthetic mineral-like supports such as spinel, metakaolinite, perovskites, hydrotalcite-, palygorskite-, and mayenite-like compounds. According to literature, metakaolin has irregular amorphous alumina surfaces that could be covalently grafted with compounds to form hybrid materials with high chemical and thermal stability [22-25]. The main constituents of metakaolin are SiO_2, and Al_2O_3, with minor content of Fe_2O_3, CaO and TiO_2, which are common respective carrier materials. These oxides are responsible for improve metal dispersion, reduce particle sintering, increase thermal stability and enhance oxygen storage capacity [26]. Mixed oxides-supported catalyst enable the formation of spinels ($MgAl_2O_4$ and $NiAl_2O_3$), which could keep nickel in its active form and exhibit moderate acidic and basic site strength and density compared to pure oxides supported catalyst, reducing the tendency of by-products formation [17, 13]. In this regard, this research work focusses on synthesis and characterization of MgO-doped/acid modified metakaolin supported Ni catalysts for ethanol steam reforming. The dehydroxylation of the metakaolin would increase its Si/Al ratio and in turn improve the activity and selectivity of the catalyst. The essence of the study and composition of the catalysts is to verify their physicochemical properties that would be applicable for ethanol steam reforming, with tendency for the reduction of by-products formation.

2. Materials and Methods

2.1. Catalyst Preparation

Acid modified metakaolin supported nickel-based catalysts were synthesized by wet impregnation method for ethanol steam reforming reaction in the vapour phase. Metakaolin was dispersed in 6 M H_2SO_4 at a solid/liquid ratio of 1:20 by weight for 6 h under stirring and refluxed at 70°C. After cooling, the mixture was filtered and the residue was dried in an oven at 90°C for 6 h. The modified metakaolin was oxidized by dipping it in a saturated solution of ammonium cerium (IV) nitrate in 2 M H_2SO_4 in a proportion of 1 g of activated metakaolin per 10 ml of solution and the resulting mixture was filtered, washed with hot distilled water to attain pH of 7 and then dried. The loading of nickel on the respective supports (2g) ranged from 5-25 wt %, using 1 g of magnesium oxide and nickel nitrate hexahydrate in 50 mL (39.5g) of ethanol and stirred in a beaker at 250 rpm for 1 h. The slurry was dried in a rotavapour at 75°C under vacuum and then calcined in air at 650°C for 3 h (modified method of

Olivares et al. [27]).

2.2. Catalyst Characterization

Thermogravimetric / differential thermal analyses (TG/DTA) were performed with a Perkin Elmer STA 4000 instrument. 15 mg of sample was put into a ceramic pan placed in integrated furnace in the equipment and heated from room temperature to 950°C at a constant heating rate of 10°C / min, operating in a stream of nitrogen gas flow at 20 ml/min and pressure of 2.5 bar. The traces were recorded as weight loss/derivative weight loss versus temperature for TG/DTA respective graphs.

X-ray powder diffraction (XRD) analysis was used to find out the crystalline phases and calculate mean crystallite size in the calcined catalysts. The XRD data were obtained at ambient temperature using a Diffractometer system-EMPYREANr with Cu Kα radiation and operated at 45 kV and 40 mA. X-ray diffraction patterns were recorded within the 2θ range of 10 to 70° with a scan speed of 0.026° in 2θ / step, and counting time/step of 1 s. The crystallite size was calculated by the Scherrer equation:

$$D = k\lambda/\beta\cos\theta$$

where D is the mean crystallite size (nm), k is a dimensionless shape factor with a typical value of about 0.9, λ is the x-ray wavelength, β is the line broadening at half the maximum intensity (FWHM) (in radian equivalent) and θ is the Bragg angle (in radian equivalent).

The x-ray fluorescence (XRF) analyses of samples were done using Thermo Scientific Niton Analyzer-XL3t 950 and scintillation detector with a current (40 mA) and voltage (60 kV). 1 g of the samples were analysed for 60 s and the result was obtained and recorded.

FTIR spectra were recorded using Perkin-Elmer Infrared spectrophotometer and KBr pellets with resolution of 4 cm^{-1}, in the range of 450-4000 cm^{-1}. The sample and analytical grade KBr were dried at 100°C overnight prior to the FTIR analysis.

Nitrogen adsorption-desorption isotherms measurements (Brunauer-Emmet-Teller method) were performed at liquid nitrogen temperature of -196°C using Quantachrome NovaWin instrument (version 11.03). Before each measurement, the samples were outgassed at 250°C for three hours prior to the analysis. Isotherms points in the P/P0 = 0.05–0.10 range were used to calculate the multi-point BET specific surface area. The total pore volume calculation was based on nitrogen volume at the highest relative pressure, whereas the average pore size diameter was calculated by the Barrett-Joyner-Halenda (BJH) method.

Scanning electron micrographs were taken on a JEOL-JSM 5600LV microscope, equipped with a 6587 EDX (Energy dispersive x-ray spectrometry) detector, using an accelerating voltage of 15 kV. The samples were deposited on a sample holder with an adhesive carbon foil and sputtered with gold.

3. Results and Discussion

3.1. Catalyst Formulations

In the formulations, the nickel contents were varied as follows: 0%, 5%, 10%, 15%, 20% and 25% relative to the total weight of the synthesized catalyst. The catalyst MKMgO-C (CAT-Blank) corresponds to the pure catalytic support (modified metakaolin) and promoter (MgO) (without nickel, Ni 0%), while prepared supported catalysts with 5%, 10%, 15%, 20% and 25% wt% Ni loadings and MgO were named as 5Ni-MgO-modified metakaolin (CAT I), 10Ni-MgO-modified metakaolin (CAT II), 15Ni-MgO-modified metakaolin (CATIII), 20Ni-MgO-modified metakaolin (CATIV) and 25Ni-MgO-modified metakaolin (CAT V) catalysts, respectively.

3.2. Supported-Catalysts Characterizations

The thermal stability, textural property, crystallographic structure, chemical composition, morphology/phase composition and nature of chemical bonds of the MgO-doped/acid modified metakaolin supported nickel-based synthesized catalysts were characterized using TG/DTA, BET, XRD, XRF, SEM/EDSX and FTIR, respectively.

3.2.1. The Textural Properties of Calcined Supported Catalyst Samples

The textural properties of the calcined supported catalysts were determined by N_2 adsorption-desorption isotherms at 77 K. Specific surface area (SBET) was calculated by Brunauer-Emmett-Teller (BET) method, cumulative pore volume (Vp) and average pore diameter (Dp) were respectively calculated from Barrett-Joyner-Halenda (BJH) desorption isotherm. The calculated values are as presented in Table 1.

Table 1. *Textural properties of calcined catalysts.*

Samples	SBET (m^2/g)	Vp (cc/g)	Dp (nm)
Blank- CAT	471.70	0.2613	2.123
CAT I	434.90	0.2704	2.144
CAT II	456.10	0.2524	2.133
CAT III	635.50	0.3503	2.122
CAT IV	475.10	0.2434	2.153
CAT V	574.50	0.2807	2.108

B-CAT served as control sample for the experiment, and possessed a sizeable specific surface area and pore diameter. This could be ascribed to the doping of metakaolin with MgO, which induces more pores to the structure of the composite [17]. Pavlova et al. [14] reported that dispersion of Ni on mesoporous support provides control of the Ni particle size and prevents sintering under reaction conditions owing to a confinement of the metal particles within structured pore, thus ensuring high catalyst stability. It has been reported that the addition of MgO to Ni-metakaolin supported catalysts resulted in good metal dispersion on the catalyst surface, increase in basicity, specific surface area and pore volume, due to the formation of $MgAl_2O_4$ spinel phase or NiO-MgO solid solutions [17]. Khairudin et al. [28] reported that MgO characteristic such as high thermal stability, high melting point

and low cost make it promising component in endothermic reactions, especially in ethanol steam reforming process.

CAT I has specific surface area, pore volume and pore diameter as 434.9 m^2/g, 0.2704 cc/g and 2.144 nm, respectively. As the Ni loading increases from 5% in CAT I, the specific surface areas and pore volumes of CAT II, CAT III correspondly increase, and then decrease against CAT IV. This could be due to the aggregation and formation of crystallite nickel oxide cluster, resulted from the addition, could have blocked the pores of the catalyst and caused resultant decrease in specific surface area and pore volume [29, 30]. Secondly, metal Ni could be dispersed unevenly on the surface, causing N_2 gas adsorbed less so that the specific surface area of the catalyst decreases with increase in Ni (wt %) [31]. CAT V subsequently increased in terms of specific surface area and pore volume, due to the dissolution of AlO_6 octahedral layers during acid treatment and proper dispersion of MgO on the outer layer of the support [32, 33]. Metal loading has a significant effect on the particle size and dispersion of the catalyst on the support, which in turn, has an effect on the catalyst activity and selectivity [34]. Although, all the catalysts have average pore diameter in the mesopore diameter range. The existence of the mesoporous structure gave the optimum pore size in aiding to adsorb the reactant gases on the catalyst's surface [35]. BET results show that the proper dispersion of active metal over the support leads to increase in specific surface area and possibly more active sites per mass of the catalysts. Dispersion of active metal over the support influences the rate of carbon deposition during reaction; the properties of the pore can control the movement of molecules related to selectivity and unique mesopores improve the mass transport and the diffusion of chemical reactant that subsequently accelerates the catalytic process. Mass transport is faster in the catalyst cavity that offers shorter diffusion pathway between the reactant and the active site of the catalyst [36-38].

3.2.2. X-ray Diffraction (XRD)

XRD provided information about the crystalline structure of the supported catalysts. The catalysts were supported with sulphuric acid modified metakaolin because catalyst with Si/Al $\geq$ 5 enhances its activity [39, 40]. The Si/Al ratio affects properties such as ion exchange capacity, thermal and hydrothermal stability, concentration and strength of acid sites of the Bronsted-type and activity and selectivity of catalysts [41]. Figure 1 shows the diffractograms of control and synthesized catalysts. All the synthesized catalysts show similar XRD patterns. The crystalline phases were identified by comparison with Joint Committee on Powder Diffraction Standards (JCPDS). The diffraction peaks of NiO particles which correspond to face centred cubic (FCC) crystalline structure, with miller indexes (hkl) at 2θ equals to 37° (111), 43° (200) and 63° (220) (JCPDS 71-1179) was observed for all the synthesized catalysts [42, 43]. Similarly, the catalysts exhibit three diffraction peaks of spinel ($NiAl_2O_4$) around 37° (311), 43° (400) and 63° (440) (JCPDS No; 10-0339). The peaks for $NiAl_2O_4$ at 37° and 43° are difficult to distinguish due to the overlap with NiO. This may be due to diffusion of NiO particles into the support structure for the formation of the nickel aluminate spinel phase [44, 45]. The presence of $NiAl_2O_4$ did not favour the deposition of carbon and metal sintering during the reaction, probably due to the greater dispersion of NiO on the catalyst surface [17, 14, 13]. There are distinguishable peaks of MgO observed in the catalysts, while most MgO are totally incorporation into the metakaolin to form $MgAl_2O_4$ spinel. This is due to the relatively high calcination temperature used in the catalyst preparation [46]. The diffraction peak characteristic of MgO was observed at 43° (JCPDS No. 98-005-6143), for all the synthesized catalysts, which reaffirm the result reported by Al-Swai et al. [17]. Three characteristic peaks were observed at 2θ ≈ 37.19° (311), 43°C (400), and 63° (018) (JCPDS No. 073-1959), corresponding to magnesium aluminate spinel phase ($MgAl_2O_4$)-for all the catalysts, as reported by Rahman and Jayaganthan [47] and Olivares et al. [27]. A characteristic peak of TiO_2 was observed at 2θ = 26.7° (JCPDS 73-1764) for all the catalysts, which corroborate with result reported by Aliyu et al. [48] and Xu and Zhang [49]. Table 2 shows the crystal sizes of NiO, calculated from the analysis of the most intense diffractions, corresponding to 2θ on average of 43°, using Debye-Scherer's equation. The large crystallite size of 132.5 nm of CAT II may be attributed to the fact that NiO particles have the tendency to agglomerate with MgO to form NiO-MgO [17]. The crystallite size of 38nm of CAT III is comparable to the crystallite size value of 35.8nm for NiO powder reported by Smoljan et al. [50]. The respective crystallite sizes of CAT I, CAT IV and CAT V as 25.6nm, 20.2nm and 20.1nm, closely collaborate with the value of 24.4nm reported by Khzouz et al. [51]. As a prerequisite in steam reforming of hydrocarbon, the reduction of NiO at high temperature would further reduced the size of the Ni metal particles to be formed for the test reaction [52]. However, size effects are observed with the reduction in size of structural elements, particles, crystallites and grains below a certain threshold. Such effect occurs at the average size of crystal grain of less than 100nm and is more clearly observed at the grain size below 10nm [53]. The crystal size influences the surface area of the catalyst, and this knowledge is very vital to surface reactions; the large crystal size may allow direct contact between the metal oxide and the catalytic support, giving good catalyst stability, favouring catalytic performance [54].

Table 2. *Crystallite size of NiO calculated through the Scherer's equation.*

Sample	Si/Al	2θ	FWHM	D (nm)[a]
CAT I	6.7	43.54	0.3149	25.6
CAT II	13.7	43.03	0.059	132.5
CAT III	8.6	43.00	0.2362	33.8
CAT IV	5.7	43.35	0.3936	20.2
CAT V	6.7	43.51	0.3936	20.1

[a] calculated by using the (200) NiO plane.

3.2.3. Scanning Electron Micrographs / Energy Dispersive X-ray Spectrometry (SEM/EDX)

The SEM technique was used to examine the catalysts' surface texture and morphology. The SEM images of calcined catalysts are as shown in Figure 2 (a-f). The calcined catalysts

are of uniform morphology. The images show that the supported catalysts are formed from mesoporous agglomerates of homogeneous sized particles with a spherical and plate-like shape [55]. The particles agglomerate formed on the catalysts is ascribed to the nuclear interaction between MgO and NiO in the formation of NiO-MgO [17]. SEM images show that metal particles with spherical shapes are randomly distributed on comparatively larger irregular shaped metakaolin-supported Ni-based catalysts; it was observed that the metal particles are uniformly dispersed on support particles [56]. EDX microanalysis was used to characterize the elemental composition of the synthesized catalysts. EDX results show that nickel is well dispersed and prevalent on the surface of the catalysts, including minor elements. The major elements present in the catalysts at different proportions are Fe, Ni, Ti, Si, Al, Zn, Mg, and Ca, which corroborate with Ni-based catalysts results published by Aliyu et al. [48] and El-Alouani et al. [57]. The synergistic effect among the elemental and oxide composition may lead to better catalytic performance of the synthesized catalysts [58, 59].

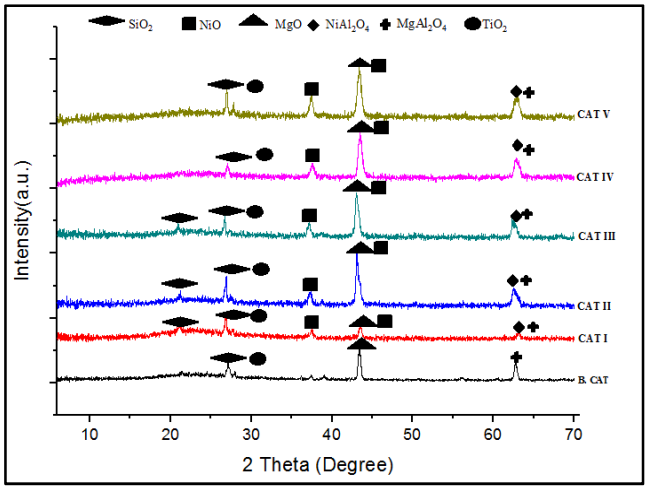

Figure 1. *XRD pattern of the control and synthesized catalysts at 25°C and 1 atm (K-α = 1.54).*

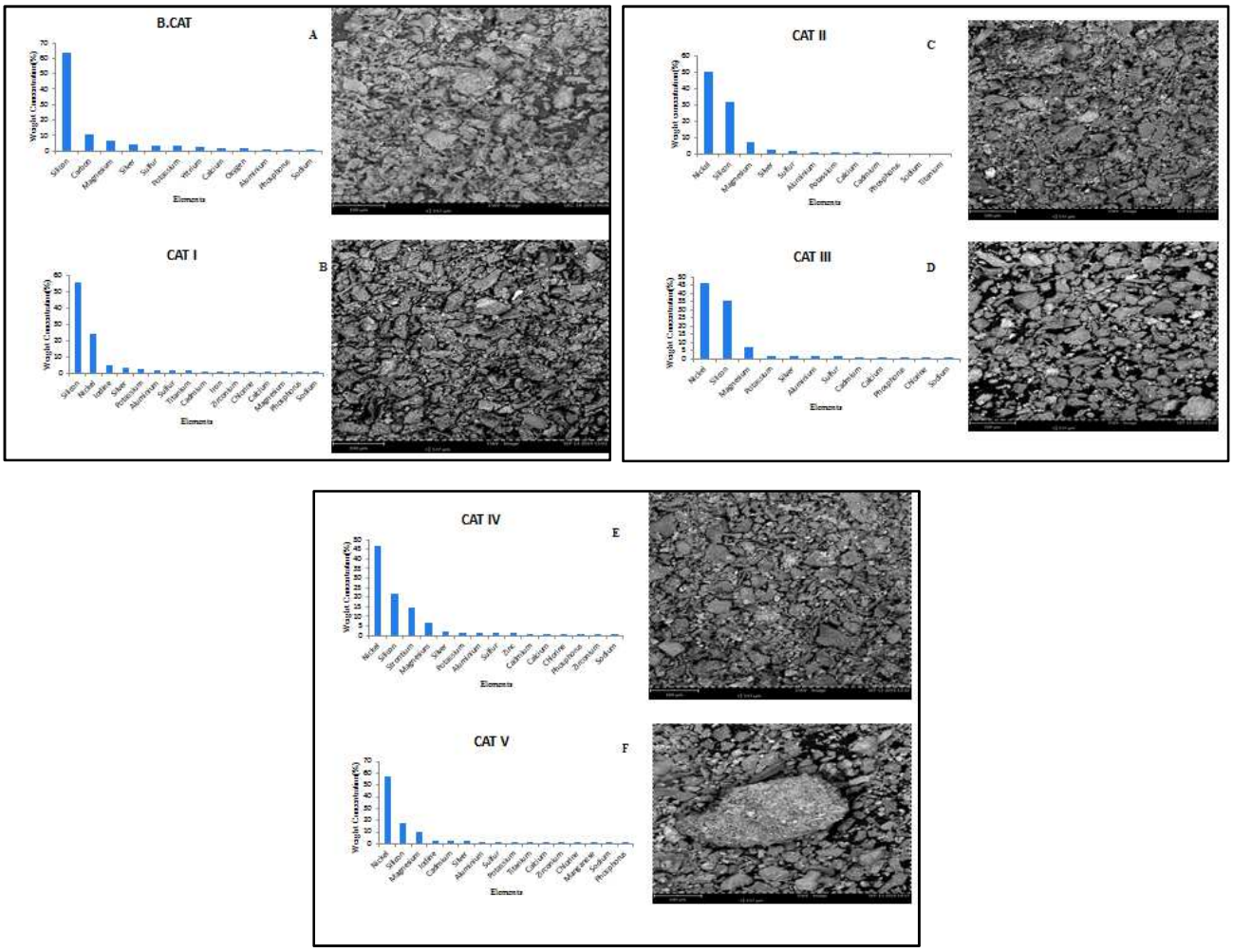

Figure 2. *SEM micrograph of (a) B. CAT (b) CAT I (c) CAT II (d) CAT III (e) CAT IV (f) CAT V catalysts with corresponding EDX spectrum and weight percentage using FOV: 537µm and mode: 15kV.*

3.2.4. Fourier Transform Infrared (FTIR)

The metal-support bonds in calcined catalysts of acid modified-metakaolin supported nickel-based catalysts and associated functional groups were investigated using FTIR technique. The spectra were recorded using KBr wafers in

the frequency range of 4000-400 cm^{-1}, as shown in Figure 3. The IR spectra can commonly provide useful information on the surface modification of the metakaolin and calcined catalysts. In the range, vibration of the adsorption profile that characterized interactions can be observed. The band assignment has been made by comparison with the data reported in the literature for metakaolin and calcined catalysts, as tabulated in Table 3. The FTIR spectrum of the catalyst exhibited characteristic peak and shoulder at approximately 1099 and 1200cm^{-1}, which are assigned to stretching vibrations of the three-dimensional Si-O-Si network. According to literature, vibration at about 550 cm^{-1} are attributed to Si-O bonds [60]. The band at about 660 cm^{-1} is attributed to the presence of nickel phyllosilicate bonds which covered the surface of the calcined catalysts, which is present in all the catalyst samples. The adsorption peaks recorded at 400-600 cm^{-1} could be considered to be of Zn-O stretching, which is present in all the synthesized catalyst samples [61]. The stretching vibration of the Si-O-Si network was also observed through a weaker peak at 794.7 cm^{-1}. Bands which exist between 532 and 757 cm^{-1} correspond to stretching vibrations of Si-O-Al. Absorption band at 1647.26 cm^{-1}, which is attributed to the distorted OH groups stretching vibration is present in all the synthesized catalysts. The band at 451.36 cm^{-1} is attributed to the Ti-O-Ti stretching vibration [49]. The adsorption peaks at 3406.4 cm^{-1} could be attributed to the OH stretching vibration [62]. The broad bands around 3400 and 1620 cm^{-1} are due to the adsorbed water [63]. The bands at 3385 and 1635 cm^{-1} were attributed to O-H bending, which can be due to physically adsorbed water. The vibrations of hydroxyl groups comprise the O-H stretch derived from two contributions: (i) non-dissociated O-H species and (ii) O-H species (dissociated from water), both adsorbed. The 1300 cm^{-1} region is related to the OH group present on the surface, and the region below 1000 cm^{-1} is characterized by metal-oxygen bonds [54]. The FTIR results show the presence of stretching vibrations of Si-O-Al, nickel phyllosilicate bonds (-O-Ni-O-Si), metal-oxygen bond, and the existence of OH bonding on the surface of the calcined catalysts, which have great effect in the coordination of the atoms in the surface, leading to different properties and energetic states.

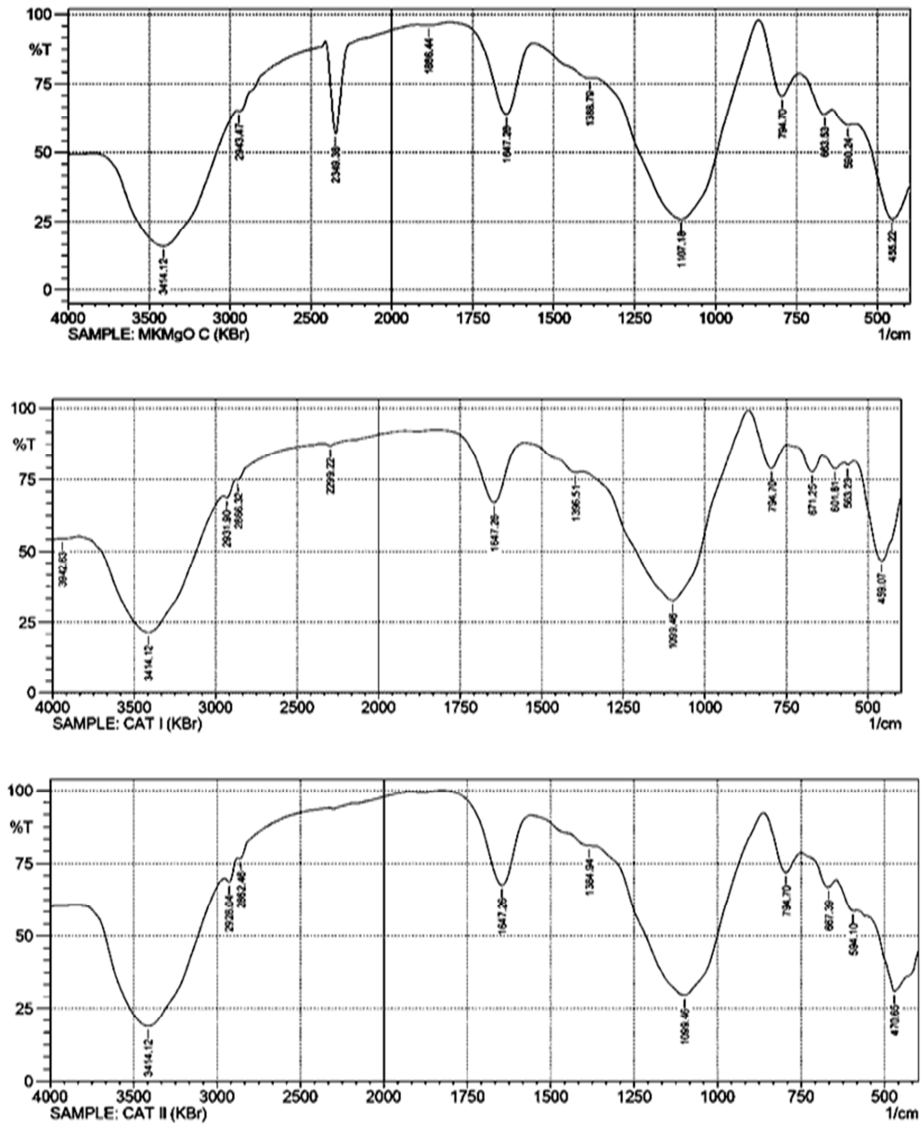

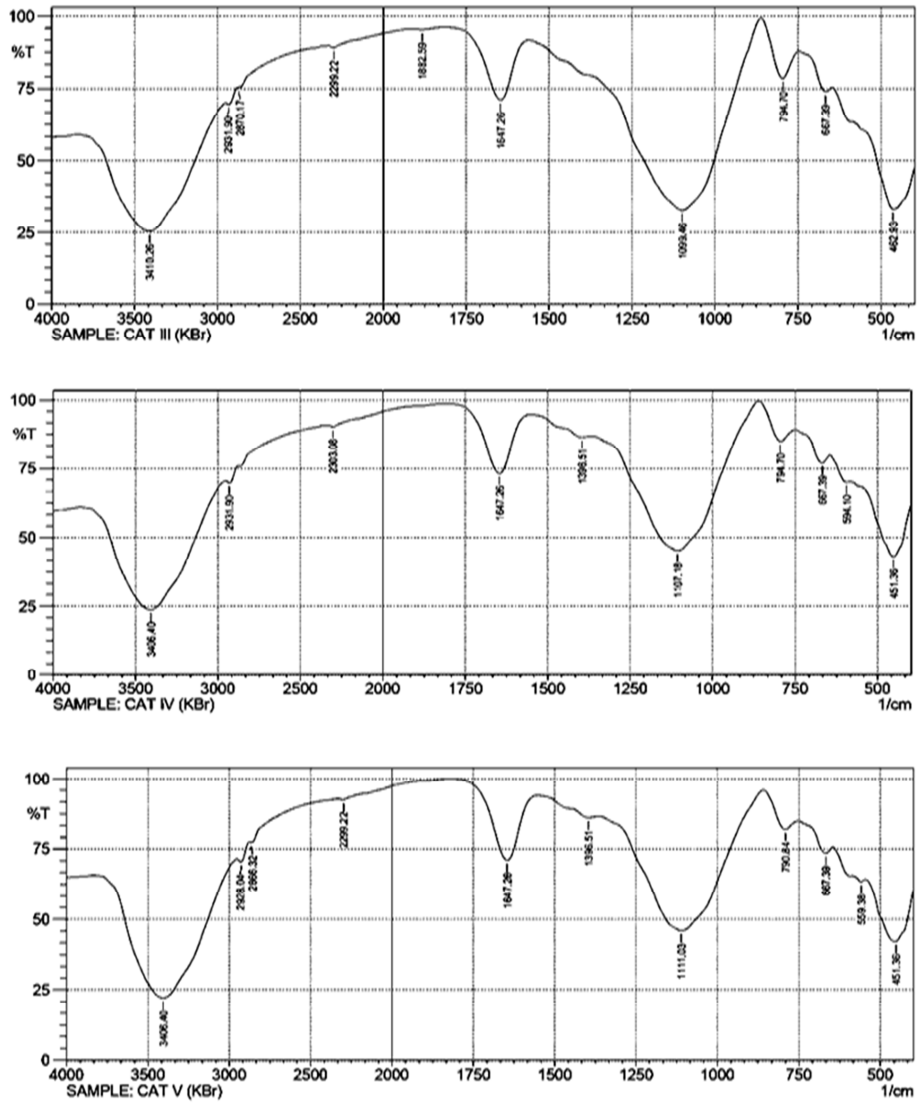

Figure 3. *FTIR spectra of control and synthesized catalysts operated at 25°C and 1 atm.*

Table 3. *Main bands identified in FTIR of investigated support, control and synthesized catalyst samples and their possible assignments.*

Bands on Support/Catalyst Samples (cm^{-1})	Bands in Literature (cm^{-1})	Assignments	References
667	660	Nickel phyllosilicate bonds	[60]
1099.46	1099	Si-O-Si network	[64]
589	550	Si-O bonds	[60]
459.07, 559.38	400-600	Zn-O stretching	[61]
1647.26	1647	Distorted OH groups	[54]
3406.4	3406	OH stretching	[62]
459.07	451	Ti-O-Ti stretching vibration	[49]
3406.4	3406	Adsorbed water	[63]
559.38, 667.39	532-757	Si-O-Al stretching vibration	[64]
459.07, 559.38, 667.39 & 794.7	> 1000	Metal-oxygen bond	[54]
559.38 & 667.39	525, 685 & 705	Ni-O bonds	[65, 43]

3.2.5. Thermogravimetric / Differential Thermal Analysis (TG/DTA)

TGA was carried out to study the weight loss, thermal behaviour and structural destruction of the calcined catalysts during calcination, while the associated heat was determined using DTA. The TG curves show that there were three main weight loss regions in all the calcined catalysts (Figure 4), while the derivative thermogravimetric analyses curves are shown in Figure 5. Considering the B. CAT, the first weight region (between 26.48 and 200.18°C), arises from the bound water and volatile organic compound (5.1 wt %). The second weight loss region (38.75 wt %) between 200.18 and 373.5°C was because of crystallite formation. The endothermic DTA peaked at 480°C could be ascribed to the combustion of organic matter [66]. In this phase, the sharp drop of the curve

indicates that all the volatile components have evolved and precursor/organic matter decomposed from the heat treatment. The third weight loss region (38.75 wt %) between 373.5 and 413.5°C and with the exothermic DTA peak at 640°C, may correspond to some phase change in the catalyst sample [67]. As for CAT I, the first phase of weight loss (5.58 wt %) was in the range of 26.48-186.85°C, which could be ascribed to the evolution of chemisorbed moisture and chemicals [68]. The second and third phases of the TG/DTA of CAT I was almost the same as B.CAT in terms of weight loss, except that exothermic peak of CAT I was at 533.5°C, while that of B.CAT was at 640°C. The disparity could be due to their composition and slow decompositions of nickel phyllosilicate to the formation of nickel oxide [60]. In the TG/DTA profiles of CAT II, the first weight loss (4.0wt %) at 27-225°C region in TG together with a differential peak at around 90°C in DTA curve was probably due to the dehydration of the catalyst. The second weight loss at region of 225-372°C (82wt %) in TG accompanied with a minor endothermic peak around 589°C in DTA, could be associated with thermoxidative degradation of nickel nitrate and dehydroxylation of structural water [69, 70]. The third weight loss (5.0 wt %) between the temperature of 372°C and 545.9°C, with minor endothermic peak at 754°C, could be ascribed to phase change in catalyst sample [67]. Above 600°C, practically weight loss could not be observed any more. As for CAT III, the first region occurred between 28-278°C (3.96 wt %), with corresponding endothermic peak at 94°C in DTA curve. The weight loss is attributed to the removal of ethanol and bound water. The second weight loss region occurred at the temperature range of 278-371.64°C (39 wt %), with a steep endothermic peak at 558°C in DTA curve. The weight loss could be associated with the decomposition of nickel nitrate entrapped in the pores of the support [71]. The third weight loss (44.5 wt %) between the temperature of 371.64°C and 424.97°C, with a steep exothermic peak at 791°C, could be ascribed to phase change in catalyst sample [67]. Considering CAT IV, the first phase weight loss (10.46 wt %) was between 23-270°C, which could be attributed to removal of volatile components of the catalyst. The second phase weight loss (30 wt %) was between 270-390°C, with steep exothermic peak at 483°C. This could be attributed to the decomposition/oxidation of nitrates and precursor materials from the catalysts [56]. The third weight loss (54.5 wt %) between the temperature of 390°C and 483°C, could be ascribed to phase change in catalyst sample [67]. The temperature regions of weight losses in CAT IV are synonymous with CAT V, except that weight losses in first and third steps of CAT V were 5.5 and 50.75wt %, respectively. The TG/DTA results confirmed the absolute volatility of water, decomposition of nickel nitrate and the formation of NiO over the catalysts between 370 and 545°C. Generally, no weight loss was observed between 600°C and 800°C, suggesting that acid modified metakaolin support or catalyst is thermally stable at the designated temperatures. The calcination of the catalysts beyond 600°C would enhance the interaction between the NiO and support, as confirmed by XRD results [70].

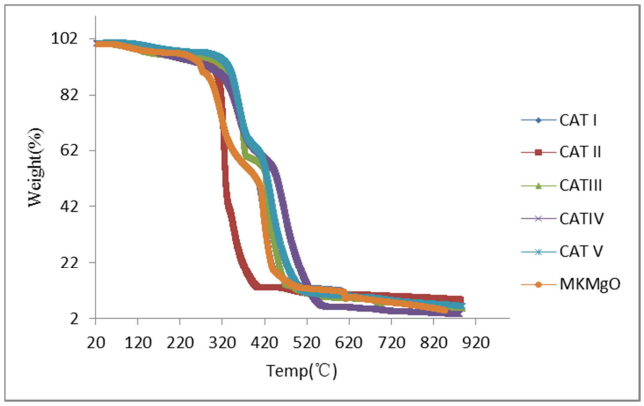

Figure 4 *TGA profiles of control and synthesized catalysts at 950°C and 2.5 bar.*

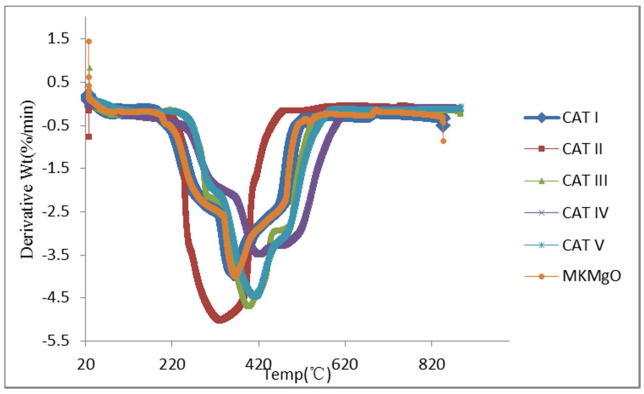

Figure 5. *DTA profiles of control and synthesized catalysts at 950°C and 2.5 bar.*

3.2.6. X-ray Fluorescence (XRF)

The chemical composition of calcined supported catalysts obtained from XRF is shown in Figure 6. The major oxides present in all the calcined catalysts are NiO, SiO_2, and Al_2O_3. Other oxides such as CaO, MgO, Fe_2O_3, TiO_2 and ZnO are present with various lower contents. CaO has high catalytic activity in different reactions and resistance to coking, while Fe_2O_3 is an active redox catalyst for a wide range of reactions, including steam reforming [72]. Petal and Patel [73] reported that addition of Fe in the formulation of catalyst improves the as-prepared catalyst's stability. Similarly, impregnation of Ni on Fe-containing mixed oxide supports can give Ni-Fe alloy particles by reduction, which in turn shows good performance in various reforming reactions in view of activity and resistance to carbon deposition [74]. TiO_2 was found to be good metal oxide catalyst support due to the strong metal support interaction, chemical stability, and acid-base property. Also, TiO_2 is used as an alternative support material for heterogeneous catalyst due to the effect of its high surface area stabilizing the catalysts in its mesoporous structure [75, 76]. Among the typical catalyst supports, silica is one of the most inert supports and is widely used in different catalytic processes. With MgO capacity for oxygen storage, it can release oxygen to oxidize the carbon formed on the catalyst surface. Another advantage of MgO as

constituent of a support or promoter in reforming arises from the possibility of formation of NiO-MgO solid solution at any molar ratio because of similar anion radii (Mg^{2+} 0.065nm, Ni^{2+} 0.072nm) and lattice parameters. Addition of basic modifiers can be efficient way for attenuating carbon formation during steam reforming reaction, by largely reducing the concentration of Lewis acid centers [77, 78]. Al-Fatesh et al. [26] reported that support made of TiO_2, Al_2O_3, SiO_2, and MgO can improve metal dispersion, reduce particle sintering, increase thermal stability, and enhance oxygen storage capacity to assist in gassifying carbon produced in reforming reaction. ZnO has better activity towards water-gas shift reaction, as it could promote the dissociation of water [79]. The loss on ignition recorded during the calcination of the catalyst samples were as a result of the adsorbed gases, organic matter, and moisture content [80]. The lower the loss on ignition value of a catalyst, the better the catalyst. XRF results show that the synergistic effect among the oxides could lead to improve metal dispersion, attenuating of carbon formation and better activity of the catalysts during the reforming reaction.

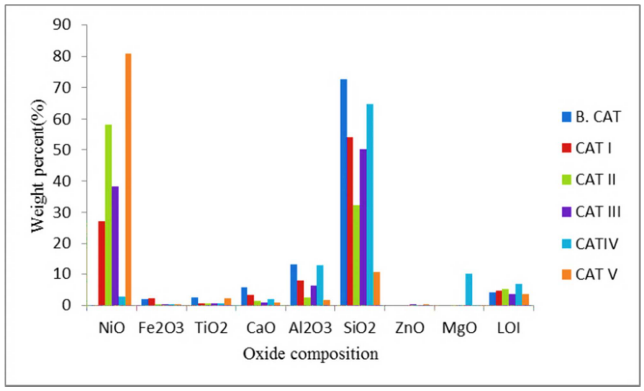

Figure 6. *Comparative oxide compositions of synthesized catalysts using XRF at 25°C and 1 atm.*

4. Conclusion

The physicochemical properties of the synthesized Ni-based catalysts based on their metal oxides and spinel structure have been studied using characterization techniques. Especially, NiO, Al_2O_3, MgO, $MgAl_2O_4$ and $NiAl_2O_4$, which are contributors to the thermal stability, activity and selectivity of the catalysts. The spinel structure in the developed catalysts would facilitate the dispersion of Ni in the reduction step prior to reaction and its mesoporous structure would fast track the adsorption of reactant gases on the catalysts surface and easy diffusion through the catalysts channel after reaction. In the same vain, MgO has high oxygen capacity which could oxidize the carbon that may be formed on the catalyst surface, and with its high melting point, it would favour stable catalyst surfaces at high reaction temperatures. The existence of OH bonding on the surface of the catalysts has great effect in the coordination of the atoms in the surface, leading to different properties and energetic states. In view of the mesoporous nature of the developed catalysts and presence of spinels like $MgAl_2O_4$ and $NiAl_2O_4$, the mass transport and diffusion of reacting gases to the active site of the catalysts would be facilitated, the thermal stability of the catalysts would be enhanced, there would be moderate acidic and basic site strength and density, and the carbon deposition would not be favoured due the presence of lattice oxygen at the catalysts' surfaces. The synthesised catalyst will be suitable for ethanol steam reforming since it can withstand high temperature.

References

[1] Rosen, M. A. and Koohi-Fayegh, S. (2016). The prospects for hydrogen as an energy carrier: an overview of hydrogen energy and hydrogen energy systems. *Energy Ecol. Environ*. 1 (1): 10-29. Doi: 10.1007/540974-016-0005-2.

[2] Dhanala, V., Maity, S. K. and Shee, D. (2015). Roles of supports (γ-Al_2O_3. SiO_2, ZrO_2) and performance of metals (Ni, Co, Mo) in steam reforming of isobutanol, *RSC Advances* 5, 52522. Doi: 10.1037/c5ra35589.

[3] Sadooghi, P. and Rauch, R. (2014). Experimental and modelling study of catalytic steam reforming of methane mixture with propylene in a packed bed reactor. International Journal of Heat and Mass Transfer 78, 515-521.

[4] Jiang, D., Fang, Z., Chin, S., Tian, X. and Su, T. (2016). Biohydrogen production from hydrolysates of selected tropical biomass wastes with clostridium butyricum, *Scientific Reports* 6: 27205. Doi: 10.1038/srep27205.

[5] Sathyanarayanan, S. V. (2014). Biological hydrogen production from lignocellulosic biomass in an up-flow anaerobic sludge blanket reactor using mixed microbial cultures. *Electronic Theses and Dissertations paper* 5088.

[6] Wang, Y., Zou, S., and Cai, W. B. (2015). Recent Advances on Electro-oxidation of ethanol on Pt- and Pd-based catalysts from reaction mechanisms to catalytic materials. *Catalysts* 5, 1507–1534.

[7] Gaudillere, C., González, J. J., Chica, A. and Serra, J. M. (2017). YSZ monoliths promoted with Co as catalysts for the production of H_2 by steam reforming of ethanol. Applied Catalysis A: General 538, 165–173.

[8] Moller, K. T., Jensen, T. R., Akiba, E. and Li, H. (2017). Hydrogen- A sustainable energy carrier. Progress in Natural Science: Materials International 27, 34-40.

[9] Isah, N. A., Eterigho, E. J., Olutoye, M. A., Garba, M. U. and Okokpujie, I. P. (2020). Development and test performance of heterogeneous catalysts on steam reforming of bioethanol for renewable hydrogen systhesis: A review. Journal of Advanced Research in Fluid Mechanics and Thermal Sciences 73 (1), 69-108. https://doi.org/ 10.37934/ arfmts.73. 1.69108.

[10] Nabgan, W., Tuan Abdullah, T. A., Mat, R., Nabgan, B., Gambo, Y., and Triwahyono, S. (2016). Influence of Ni to Co ratio supported on ZrO_2 catalysts in phenol steam reforming for hydrogen production. International Journal of Hydrogen Energy 41, 22922–22931.

[11] Dan, M., Mihet, M., Lazar, M. D., and Muresan, L. M. (2016). Promoted alumina supported Ni catalyst for ethanol steam reforming. Studia Ubb Chemia, LXI, 2, 137-154.

[12] Konsolakis, M., Loakimidis, Z., Kraia, T. and Marnellos, G. E. (2016). Hydrogen production by ethanol steam reforming over CeO_2 supported transition metal (Fe-Co, Ni, Cu) catalysts: Insight into the structure –activity relationship. Catalysts 6, 39.

[13] Thyssen, V. V, Maia, T. A. and Assaf, E. M. (2015). Cu and Ni catalysts supported on γ-Al_2O_3 and SiO_2 assessed in glycerol steam reforming reaction. Journal of the Brazilian Chemical Society, vol. 26, no. 1, 22-31.

[14] Pavlova, S., Fedorova, Y., Ishchenko, A., Melgunov, M., Melggunova, E., Simonov, M., Rgov, V., Kniger, T., Sadykov, V. and Roger, A. (2018). Ni-containing catalysts based on ordered mesoporous MgO-Al_2O_3 for methane reforming. Catal. Sustain. Energy 5, 59-66. https://doi.org/10.1515/cse.2018-0008.

[15] Mezalira, D. S, Probst, L. D., Pronier, S., Batonneau, Y., Batiot-Dupeyrat, C. (2011). Decomposition of ethanol over Ni/Al_2O_3 catalysts to produce hydrogen and carbon nanostructured materials. Journal of Molecular Catalysis A: Chemical, 340, 15-23. DOI: 10.1016/j.molcata.2011.03.013.

[16] Lu, M., Xiong, Z., Fang, K., Li, J., Li, X. and Li, T. (2020). Effect of promoters on steam reforming of toluene over a Ni-based catalyst supported on coal gangue ash. ACS Omega 5, 41, 26335-26346. https://doi.org/10.1021/acsomega.oc01197.

[17] Al-Swai, B. M., Osman, N. B. and Abdullahi, B. (2017). Catalytic performance of Ni/MgO catalyst in methane dry reforming. AIP Conference Proceedings 1691, 020028. Retrieved on 28/10/2019 from https://aip.scitation.org/doi/pdf/10.1063/1.5005361

[18] Cifuentes, B., Figueredo, M., and Cobo, M. (2017). Response surface methodology and aspen plus integration for the simulation of the catalytic steam reforming of ethanol. Catalysts, 7 (1), 15. https://doi.org/10.3390/catal7010015.

[19] Grzybek, G., Grehik, M., Tarach, K., Pyra, K., Slowik, G., Rotko, M. and Gora-Marek, K. (2020). Bioethanol steam reforming over cobalt-containing USY and ZSM-5 commercial zeolite catalysts. Frontiers in Materials 7: 597528. Doi. 10.3389/fmats.2020.597528.

[20] Lee, S., Shin, S., Baek, H., Choi, Y., Hyun, K., Seo, M., Kim, K., Koh, D., Kim, H. and Choi, M. (2020). Dynamic metal-polymer interaction for the design of chemoselective and long-lived hydrogenation catalysts. Science Advances 6: eabb7369. Doi: 10.1126/sciadv.abb7369.

[21] Taher, N. M., Mahmoudi, M., and Sajjadivand, S. S. (2017). Cobalt catalysts preparation and characterization over alumina supported for Fischer Tropsch synthesis. Biofuel Eng 2, 51-61. Retrieved on 18/1/2019 from https://doi.org/10.1515/bfuel.2017-0004.

[22] Zhang, Z., Liu, L., Shen, B. and Wu, C, (2018). Preparation, modification and development of Ni-based catalysts for catalytic reforming of tar produced from biomass gasification. Renewable and Sustainable Energy Review, 94, 1086-1109. https://doi.org/10.1016/jirser.2018.07.010

[23] Rahayu, E. S., Subiyanto, G., Imanuddin, A., Wiranto, Nadina, S., Ristiani, R., Suhermina, and Yuniarti, E. (2018). Kaolin as a source of silica and alumina for synthesis of zeolite Y and amorphous silica alumina. MATEC Web of Conferences 156, 05002.

[24] Zhang, S., Liu, Q., Gao, F., Li, X., Liu, C., Li, H., Boyd, S. A., Johnson, C. T. and Teppen, B. J. (2017). Mechanism association with kaolinite intercalation with urea: combination of infrared spectroscopy and molecular dynamics simulation studies. Journal of Phys. Chem. Nanomater Interfaces 121 (1), 402-409.

[25] Worasith, N., Goodman, B. A. and Deng, W. (2018). Formation of new low field signals in the EPR spectra of kaolin minerals. The Journal of Applied Science 17 (1), 12-18.

[26] Al-Fatesh, A. S., Kasim, S. O., Ibrahim, A. A., Fakeeha, A. H., Abasaeed, A. A., Alrashedd, R., Ashamari, R. and Bagabas, A. (2019). Combined magnesia, ceria and nickel catalyst supported over γ-alumnia doped with titania for dry reorming of methane. Catalysts 9, 188. Retrieved on 30/10/19 from https:// www.mdpi.com/journal/catalysts.

[27] Olivares, A. C. V., Gomez, M. F., Barroso, M. N. and Abello, M. C. (2018). Ni-supported catalysts for ethanol steam reforming: effect of the solvent and metallic precursor in catalyst preparation. International Journal of Industrial Chemistry 9, Issue 1, 61-73.

[28] Khairudin, N. F., Sukri, M. F. F., Khavarian, M. and Mohammed, A. (2018). Understanding the performance and mechanism of Mg-containing oxides as support catalysts in the thermal dry reforming of methane. Beilstein Journal of Nanotechnology 8, 1162-1183.

[29] Arevalo, J. D., Martinez, A., Varges, J. and Cordoba, I. F. (2018). Hydrogen production and purification of bioethanol steam reforming and preferential oxidation of CO. TECCIENCA, 13 (25), 55-64.

[30] Schmtt, C. C, Reolon, M. B. G., Zimmermann, M., Raffelt, K., Grunwaldt, J. and Dahmen, N. (2018). Synthesis and regeneration of nickel-based catalysts for hydrodeoxygenation of beech wood fast pyrolysis bio-oil. Catalysts, 449. Retrieved on 28/11/2019 from www.mdpi. com/ journal/catalysts

[31] Dewajani, H., Rochmadi, Purwono, S., and Budiman, A. (2016). Effect of modification ZSM-5 catalyst in upgrading quality of organic liquid product derived from catalyst cracking of Indonesian nyamplung oil (calopyllum inophyllum). AIP Conference Proceedings 1755. 050002-1-050002-6.

[32] Blanco, P. H., Wu, C., Onwudili, J. A., and Williams, P. T. (2013). Characteirization and evaluation of Ni/ SiO_2 catalysts for hydrogen production and tar reduction from catalytic steam reforming pyrolysis-reforming of refuse derived fuel. Applied Catalysis B: Environmental, 134-13, 238-250. https://doi.org/10.1016/ j.apcatb.2013.01.016.

[33] Gaaz, T. S., Sulong, A. B., Kadhum, A. AA. H, Nassir, M. H. and Al-Amiery, A. A. (2016). Impact of surfuric acid treatment of halloysite on physic-chemic property modification. Materials (Basel), 9 (8): 620. Doi: 10.3390/ma9080620.

[34] Akbarzadeh, O., Zabidi, N. A. M., Abdulwahab, Y., Hamizi, N. A,, Chowdhury, Z. Z, Merican, Z. M. A., Ab-Rahman, M., Akhter, S., Shalauddin, M. and Johan, M. R. (2018). Effect of cobalt loading, particle size, and calcination condition on Co/CNT catalyst performance in Fischer-Tropsch reactions. Symmetry 11, 7, 1-18.

[35] Derekaya, F. B. and Kilinc, Y. S. (2018). The CO methanation over the Rh and Ru promoted NiO-CeO_2-ZrO_2 catalysts. *Journal of Science* 31 (4), 1064-1077.

[36] Wang, F. Hao, G., Guo, Y., Ma, X. and Yang, L. (2017). Solvent effect on preparation of Pd-based catalysts: Influence on properties of palladium and its catalytic activity for benzyl alcohol oxidation. *Open Journal of Metal* 7, 59-68.

[37] Qoniah, I., Prasetyoko, D., Bahruji, H., Triwahyono, S., Jalil, A. A., Suprapto, Hartiti, Purbaningtias, T. E. (2015). Direct synthesis of mesoporous aluminosilicates from Indonesian kaolin clay without calcination. Applied Clay Science 118, 290-294.

[38] Fatimah, I., Andiena, R. Z. and Yudha, S. P. (2017). Preparation of KF-modified kaolinite as green and reusable catalyst for microwave assisted biodiesel conversion. IOP Conference Series: *Materials Science and Engineering* 172 012026.

[39] Chica, A. (2013). Zeolites: Promised materials for the sutainable production of hydrogen. International Scholarly Research Notices Chemical Engineering, volume 2013, Article ID 907425 (1-9). http://dx.doi.org/10.1155/2013/907425.

[40] Kumar, S., Panda, A. K. and Singh, R. K. (2013). Preparation and characterization of acids and alkali treated kaolin clay. Bulletin of Chemical Reaction Engineering and Catalysis 8 (1), 61-69. http://dx.doi.org/10.9767/bcrec.8.1.4530.61-69.

[41] Strejcova, K., Tisler, Z., Svobodova, E., and Velvarska, R. (2020). Characterization of modified natural minerals and rocks for possible adsorption and catalytic use. Molecules 25, 4989. Doi: 10.3390/molecules25214989.

[42] Singh, S., Nga, N. T. A., Pham, T. L. M., Tan, J. S., Phuong, P. T. T. Khan, M. R. and Vo, D. V. N. (2017). Melgas production from bi-reforming of methane over La-modified santa Barbara amorphous-15 supported nickel catalyst. Chemical Engineering Transactions 56, 1573-1578.

[43] Moavi, J., Buazar, F. and Sayahi, M. H. (2021). Algal magnetic nickel oxide nanocatalyst in accelerated synthesis of pyridopyrimidine derivatives. *Scientific Reports*, 11, 6296. https://doi.org/10.1038/841598-021-85832-z

[44] Ramesh, S. and Venkatesha, N. J. (2017). Template free synthesis of Ni-perovskite: An efficient catalyst for hydrogen production by steam reforming of bioglycerol. *ACS Sustainable Chemistry and Engineering*, 5, 1339-1346. https://doi.org/10.1021/acssus chemeng.6601744.

[45] He, L., Ren, Y., Yue, B., Tsang, S. C. E and He, H. (2021). Tuning metal-suppoort interactions on Ni/Al_2O_3 catalysts to improve catalytic activity and stability for dry reforming of methane. Processess, 9, 706. https://doi.org/10.3390/pr9040706.

[46] Alvarez-Galvari, C., Melian, M., Ruiz-Matas, L., Eslava, J. L, Navaro, R. M., Ahmadi, M., Roldan Cuenya, B. and Fierro, J. L. G. (2019). Partial oxidation of methane to syngas over nickel based catalysts: influence of support type, additional rhodium and preparation method. Front Chem 7: 104. Retrieved on 28/11/2019 from http:///www.frontiersin.org/article s/10. 3389/f chem/2019.00104/full.

[47] Rahman, A. and Jayaganthan, R. (2015). Study of photo catalyst magnesium aluminate spinel nanoparticles. Journal of Nanostruct Chem, 5, 147-151. DOI: 10.1007/540097-014-0135-9.

[48] Aliyu, A., Abdukareem, A. S, Kovo, A. S., Abubakar, O. K., Tijani, J. O., and Karim, I. (2017). Synthesize multi-walled carbon nanotubes via catalytic chemical vapour deposition method oh Fe-Ni bimetallic catalyst supported on kaolin. Carbon Letters, vol 21, 33-50.

[49] Xu, J. and Zhang, T. (2019). Fabrication of spent FCC catalyst composites by loaded V_2O_5 and TiO_2 and heir comparative photocatalytic activities. Scientific Reports 9, 11099. Retrieved on 7/11/19 from https://www.nature.com/articles/s41598-019-47155-y

[50] Simoljan, C. S., Crawford, J. M. and Carreon, M. A. (2020). Mesoporous microspherical NiO catalysts for the deoxygenation of oleic acid. *Catalysis Communications* 143, 106046. https://doi.org/10.1016/j.catcom.2020.106046

[51] Khzouz, M., Du, S., Wood, J. and Gkanas, E. (2018). Catalytic performance of $Ni\text{-}Cu/Al_2O_3$ for effective syngas production by methanol steam reforming. *Fuel*, vol.232, 672-683. https://doi.org/10.1016/j.fuel.2018.06.025.

[52] Teng, C., He, J., Zhu, L., Ren, L., Chen, J., Hong, M. and Wang, Y. (2015). Fabrication and characterization of monodisperse magnetic porous nickel microspheres as novel catalysts. Nanoscale Research Letters, 10: 384. https://doi.org/10.1186/s11671-015-1088-8.

[53] Ikenyiri, P. N. & Ukpaka, O. P. (2016). Overview on the effect of particle size on the performance of wood based adsorbent. Journal of Chemical Engineering and Process Technology, 7: 315. https:/doi.org/10.4172/2157-7048-1000315.

[54] Queiroz, GA. And Barbosa, C. M. M. B. (2019). Study of the structural and morphological properties of copper catalysts supported on Al_2O_3 and TiO_2 synthesized by the impregnation method. *Revista Materia* 24 (1), 12322 (1-8).

[55] Angel-Soto, J., Martinez-Rosales, M., Angel-Soto, P. and Zamorategui-Molina, A. (2017). Synthesis, characterization and catalytic application of Ni catalysts supported on alumina-zirconia mixed oxides. Bull. Materials Science 40 (7), 1309-1318.

[56] Mondal, T., Pant, K. K. and Dalai, A. K. (2015). Catalytic oxidative steam reforming of bio-ethanol for hydrogen production over Rh promoted $Ni/CeO_2\text{-}ZrO_2$ catalyst. *International Journal of Hydrogen Energy* 40, 2529-2544.

[57] El-Alouani, M., Alehyen, S., El-Achouri, M., and Taibi, M. (2019). Preparation, characterization, and application of metakaolin-based geopolymer for removal of methylene blue from aqueous solution. Journal of Chemistry, vol.2019, Article ID 4212901, 1-14. Retrieved on 16/11/2019 from downloads.hinddwi.com/journals/jschem/2019/4212901.pdf

[58] Xian, G., Zhang, N., Zhang, G., Zhang, Y. and Zou, Z. (2019). FeNiCeOx ternary catalyst prepared by ultrasonic impregnation method for diclofenac removal in fenton-like system. Water Science and Technology 79 (9), 1675-1684.

[59] Levent, M., Agbaba, M. and Sahin, Y. (2016). Production of synthesis gases from ethanol steam reforming process. International Journal of Clean Coal and Energy 5, 45-63.

[60] Hermida, L., Abdullah, A. Z. and Mohammed, A. R. (2018). FT-IR and TGA of MCF silica-supported nickel catalyst. *Journal of Materials and Environmental Sciences* 9 (8), 2328-2333.

[61] Arana, J. T., Torres, J. J, Acevedo, D. F., Illanes, C. O, Ochoa, N. A. and Pagliero, C. L. (2019). One-step synthesis of CaO-ZnO efficient catalyst for biodiesel production. International Journal of Chemical Engineering, vol. 2019, Article ID 1806017, 1-7.

[62] Yu, L., Song, M., Wei, Y. and Xiao, J. (2018). Combining carbon fibers with Ni/γ-Al_2O_3 used for syngas production (Part A): preparation and evaluation of complex carrier catalysts. *Catalysts* 8 (12), 658. Retrieved on 7/11/2019 from https://www.mdpi.com/2073-4344/8/12/658/htm

[63] Mbaye, A., Diop, C. A. K., Miehe-Brendle, J., Senocq, F. and Muary, F. (2014). Characteization of natural and chemically modified kaolinite from Mako (Senegal) to remove lead from aqueous solutions. Clay Minerals 49 (4), 527-539.

[64] Mgbemere, H. E., Lawal, G. I. Ekpe, I. C. and Chaudhary, A. I. (2018). Synthesis of zeolite-A using kaolin samples from Darazo, Bauchi state and Ajebo, Ogun state in Nigeria. Nigerian Journal of Technology 37 (1), 87-95.

[65] Ebin, B. (2018). Simple preparation of Ni and NiO nanoparticles using raffinate solution originated from spent NiMH battery recycling. *Journal of Inorganic and Organometallic Polymers and Materials*, 28, 2554-2563. https://doi.org/10.1007/ s10904-028-0926-4

[66] Ding, Y. Zhang, H. Li, J., Zhang, S., Liu, B., Ekberg, C. and Jian, Z. (2019). Recovery of platinum from spent petroleum catalysts: Optimizatio using response surface methodology. Metals, 9, 354. Doi.: 10.3390/met9030354.

[67] Patil, B., Sharma, S., Mohanta, H. K. and Roy, B. (2017). BINIVOX catalyst for hydrogen production from ethanol by low temperature steam reforming (LTSR). *J. Chem. Sci*, 129 (11), 1741-1746. https://doi.org/10.1007/s12039-017-1388-x.

[68] Sharma, S., Patil, B., Pathak, A., Ghosalkar, S., Mohanta, H. K., and Roy, B. (2017). Application of BICOVOX catalyst for hydrogen production from ethanol. Chem. Techn. Environ Policy, 20, 695-701. https://doi.org/10.1007/s10098-017-1394-1.

[69] Prajitha, P. M. K. and Pushpaletha, P. (2017). Preparation of solid acid catalyst from modified kaolinite and its characterization and catalytic activity. *Indian Journal of Chemical Technology* 24, 637-643.

[70] He, S., Zhang, L., He, S., Mo, L., Zhang, X., Wang, H. and Luo, Y. (2015). Ni/SiO_2 catalyst prepared with nickel nitrate precursor for combination of CO_2 reforming and partial oxidation of methane: Characterization and deactivation mechanism investigation. Journal of Nanomaterials, V2015, Article ID 659402, 1-8. http://dx.doi.org/10.1155/2015/659402.

[71] Zangouei, M., Moghaddan, A. Z and Arasteh, M. (2010). The influence of nickel loading on reducibility of NiO/Al_2O_3 catalysts synthesized by sol-gel method. Chemical Engineering Research Bulletin 14, 97-102. https://doi.org/10.3329/cerb.v14i2.5052.

[72] Al-Zeer, M. I. M. and Mackenzie, K. J. D. (2019). Fly ash-based geopolymers as sustainable bifunctional heterogeneous catalysts and their reactivity in Friedel-crafts acylation reactions. *Catalysts* 9 (4). 372. Retrieved on 12/11/2019 from https://www.mdpi.com /2073-4344 /9/4/372/htm.

[73] Petal, R. and Patel, S. (2015). Renewable hydrogen production from butanol: a review. Clean Energy 1 (1), 90-101.

[74] Tomishige, K., Li, D., Tamura, M. and Nakagawa, Y. (2017). Nickel iron alloy catalysts for reforming of hydrocarbon: preparation, structure, and catalytic properties. *Catal. Sci. Technol*. 7, 3952-3979.

[75] Bagheri, S. Julkapli, N. M. and Abdhamid, S. B. (2014). Titanium dioxide as a catalyst support in heterogeneous catalysis. The Scientic World Journal, vol 2014. Article ID 727496, 1-21. Retrieved on 11/11/2019 from downloads.hindawi.com/journals/tswj /2014 /727496.pdf.

[76] Mulewa, W., Tahir, M. and Amin, N. A. S. (2017). Ethanol steam reforming for renewable hydrogen production over La-modified TiO_2 catalyst. *Chemical Engineering Transactions* 56, 349-354.

[77] Son, I. H., Lee, S. J., Roh, H. S. (2014). Hydrogen production from carbon dioxide reforming of methane over highly active and stable MgO promoted Co-Ni/γ-Al_2O_3 catalyst. *International Journal of Hydrogen Energy*, 39, 3762-3770.

[78] Dou, B., Wang, C., Song, Y., Chen, H., Xu, Y.(2014). Activity of Ni–Cu–Al based catalyst for renewable hydrogen production from steam reforming of glycerol. *Energy Conversion and Management*, 78, 253-259.

[79] Lin, Z., Liu, F. and He, H. (2015). Effect of preparation methods on the activity of VOx/ CeO_2 catalysts for the selective catalytic reduction of NOx with NH_3. *Catalysis Science and Technology* 5, 389-306.

[80] Yussuf, A. S., Adeniyi, O. D., Olutoye, M. A., and Akpan, U. G. (2018). Development and characterization of a composite anthill-chicken eggshell catalyst for biodiesel production from waste frying oil. International Journal of Technology, 1, 110-119. https/doi.org/10.14716/ijtech.v9i1.1166.